

Two Hg(II)-Based Macrocycles Offering Hydrogen Bonding Cavities: Influence of Cavity Structure on Heterogeneous Catalysis

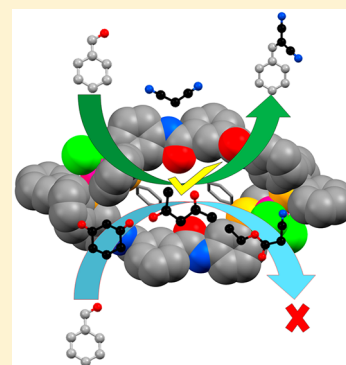
Published as part of a *Crystal Growth and Design* virtual special issue on the Structure Property Relationship in Crystalline Solids

Sanya Pachisia and Rajeev Gupta*[✉]

Department of Chemistry, University of Delhi, Delhi 110 007, India

Supporting Information

ABSTRACT: We present the synthesis and characterization of two Hg-macrocycles offering H-bonding based cavities of varying dimensions. Both Hg-macrocycles illustrate a noteworthy difference in their catalytic performance that has been related to their cavity structures.



Coordination-driven supramolecular self-assemblies are at the pinnacle of supramolecular chemistry. Such a fact is not only related to the presence of well-defined cavities such molecular assemblies offer but also due to the possibility to fine-tune these cavities.^{1–11} Several such molecular assemblies have been effectively used in host–guest chemistry,^{12–19} sensing,^{20–26} drug delivery,^{27–36} stabilizing reactive intermediates^{18,37–39} and organic transformations.^{40–53} Extensive efforts have been made to synthesize assorted molecular assemblies that show remarkable properties.^{54,55} Efforts vary from the construction of molecular assemblies offering hydrophobic interior space,^{54–57} and examples include various covalent bonding based assemblies with the objective to tune the cavity structure to suit an application. Efforts have also been made to construct metal–ligand coordination driven molecular assemblies that rely on the geometrical parameters of both metal(s) and ligand(s).^{58–60} In such molecular assemblies, the interior space has been designed to offer hydrophobic^{55,61–63} as well as hydrophilic functional groups. In contrast, examples are scarce when *hydrogen bonds* (H-bonds) are installed within a cavity.^{61–65} Such paucity is related to the difficulty in first synthetically installing H-bonds followed by giving them the required orientations to interact with an analyte of choice while also avoiding their undesirable interactions with lattice solvent molecules and/or anions.^{61,62} Although there have been a few examples where H-bonds have been incorporated within coordination-driven self-assemblies, in most cases H-bonds have been primarily used for structural purposes rather than focusing on their influence on applications.^{61–63} Our research group has recently reported two Pd(II) macrocycles

synthesized using pyridine-2,6-dicarboxamide based ligands offering appended phosphine groups.⁶⁶ Such 1 + 1 and 2 + 2 Pd-macrocycles offered inner cavity lined with H-bonds and remarkably participated in the recognition of nitroaromatics, particularly picric acid.⁶⁶

In this work, we report two discrete coordination-driven Hg(II) based molecular assemblies (**1** and **2**) synthesized using either pyridine-2,6-dicarboxamide (**L1**) or benzene-1,3-dicarboxamide (**L2**) based ligands offering appended phosphine groups. The two ligands resulted in cavities of varying dimensions therefore emphasizing the importance of pyridyl versus phenylene ring in designing contrast molecular assemblies. We also illustrate that both molecular assemblies offering H-bonds have the potential of capturing a reagent and/or substrate and such a fact has resulted in dramatic difference in their catalytic performances in the Knoevenagel condensation reactions.

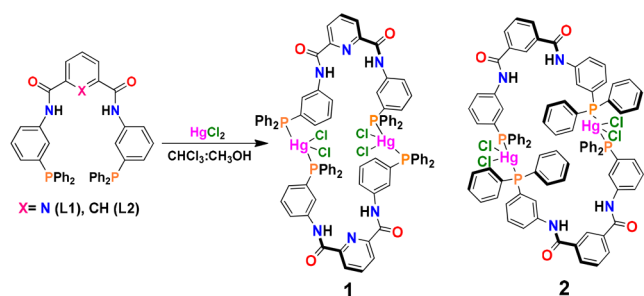
Results and Discussion. Synthesis and Characterization. Mercury macrocycles **1** and **2** were synthesized by the reaction of ligands **L1** and **L2** (Figures S1–S4, Supporting Information) with HgCl₂ in a 1:1 mixture of chloroform–methanol (Scheme 1). In both cases, a 2 + 2 self-assembly of ligands to that of Hg(II) ions was noted. Fourier transform infrared spectra of macrocycles **1** and **2** respectively revealed $\nu_{\text{C=O}}$ stretches at 1684 and 1657 cm⁻¹ (Figures S5–S6, Supporting Information) that were very similar to that of free

Received: July 28, 2019

Revised: September 13, 2019

Published: September 30, 2019

Scheme 1. Preparative Route for the Synthesis of Hg-Macrocycles 1 and 2



ligands (L1 = 1681 and L2 = 1652). Such a fact suggests that coordination to a metal ion occurs via $P_{\text{phosphine}}$ groups and not through N/O_{amidate} groups.⁶⁷ Further, broad N–H stretches were observed at 3287 and 3271 for **1** and **2** (Figures S5–S6, Supporting Information), respectively, suggesting their intact nature with however involvement in hydrogen bonding (H-bonding) interactions (vide infra).⁶⁷ Hg-macrocyclic **1** was completely insoluble in common organic solvents, whereas complex **2** was soluble in high polarity solvents such as DMF and DMSO. As a result, only Hg-macrocyclic **2** was characterized by NMR spectroscopy (Figures S7–S9, Supporting Information). The proton NMR spectrum confirms the presence of N–H resonances at 10.65 ppm (Figure S7, Supporting Information). For comparison, ligand L2 exhibits N–H signals at 10.41 ppm. Importantly, the ³¹P NMR spectrum of **2** inferred the involvement of $P_{\text{phosphine}}$ atoms in coordination to the Hg(II) ions as the ligand's phosphorus signal at –5.23 ppm was shifted to 33.91 ppm in Hg-macrocyclic **2** (Figure S9, Supporting Information).⁶⁶ Complexes **1** and **2** respectively crystallized with molecule(s) of water and DMSO, and therefore TGA was performed to evaluate their fate and to understand the thermal stability of both the complexes. For **1**, an observed weight change of ca. 7.2% (calcd. 8.3%) was noticed between 230–300 °C that corresponded to the loss of one water molecule and four Cl atoms (Figure S10, Supporting Information). In the case of **2**, a weight loss of 17.7% (calcd. 18.2%) correlated to [1 DMSO + HgCl₂] was noticed between 280–290 °C (Figure S11,

Supporting Information). Further, both Hg-macrocycles **1** and **2** start decomposing beyond ca. 320 °C.

Crystal Structures. Both Hg-macrocycles **1** and **2** were crystallographically characterized and were found to crystallize in a monoclinic cell with $C2/c$ and triclinic cell with $\bar{P}1$ space groups, respectively (Tables S1–S4, Supporting Information). The crystal structures revealed a 2 + 2 assembly of ligands to that of Hg(II) ions for both the Hg-macrocycles (Figures 1 and 2). In both cases, two Hg(II) ions are coordinated by two phosphorus atoms originating from two amide-based ligands, whereas the remaining two coordination sites are occupied by two chloride atoms. The Hg– $P_{\text{phosphine}}$ bond distances (2.4488–2.4707 Å) were very similar for two complexes, whereas Hg–Cl distances varied between 2.5184 and 2.5753 Å. The geometry around the Hg(II) ions in both macrocycles is four-coordinated. In the case of **1**, the P–Hg–P and Cl–Hg–Cl bond angles were 135.34 and 107.93°, respectively. Similarly, for complex **2**, P–Hg–P and Cl–Hg–Cl bond angles were respectively found to be 135.05 and 105.61°. In order to understand the geometry being deviated from a perfect tetrahedral ($\tau_4 = 1$) and a perfect square-planar ($\tau_4 = 0$), a four-coordinate geometry index, τ_4 , was calculated for both complexes. Hg-macrocycles **1** and **2** respectively showed τ_4 values of 0.82 and 0.81, suggesting predominantly tetrahedral geometry around the Hg(II) ions.⁶⁸

Both Hg-macrocycles exhibited remarkable structural features including H-bonds and cavities of varying dimensions. In Hg-macrocyclic **1**, pyridine-2,6-dicarboxamide based fragments are oriented in syn fashion, and as a result H-bonding groups are directed within the macrocyclic cavity. Such a structural feature is due to the presence of a pyridine ring that has aligned both amide fragments in a single orientation.⁶⁹ In addition, two lattice water molecules were found to be located within the pyridine-2,6-dicarboxamide fragment based cavities and formed H-bonds both with N–H and N_{pyridine} groups: N2–H2...O1W = 2.939 Å, N3–H3...O1W = 2.932 Å, and N1...H–O1W = 3.075 Å. A hydrogen atom of water molecule, O1W, further makes an H-bond with the Hg-bound Cl atom with a bond distance of 3.114 Å. Such an H-bonding is assisted by the fact that both Cl atoms are facing inward toward the interior of the macrocycle. Two Hg(II) ions are coordinated by

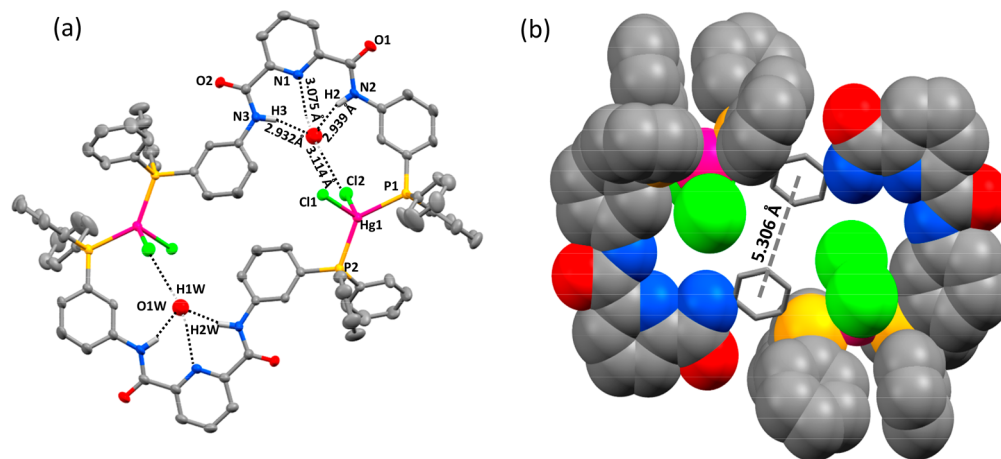


Figure 1. (a) Crystal structure of Hg-macrocyclic **1** where thermal ellipsoids are drawn at the 30% probability level, and hydrogen atoms, except for N–H groups, have been omitted for clarity. Selected bond distances (Å) and bond angles (deg): Hg1–P1, 2.4707(11); Hg1–P2, 2.4617(11); Hg1–Cl1, 2.5184(12); Hg1–Cl2, 2.5612(13); P2–Hg1–P1, 135.34(4); Cl1–Hg1–Cl2, 107.93(4). (b) Space-fill model of **1** where arene rings bound to the amide groups are shown in a capped stick fashion.

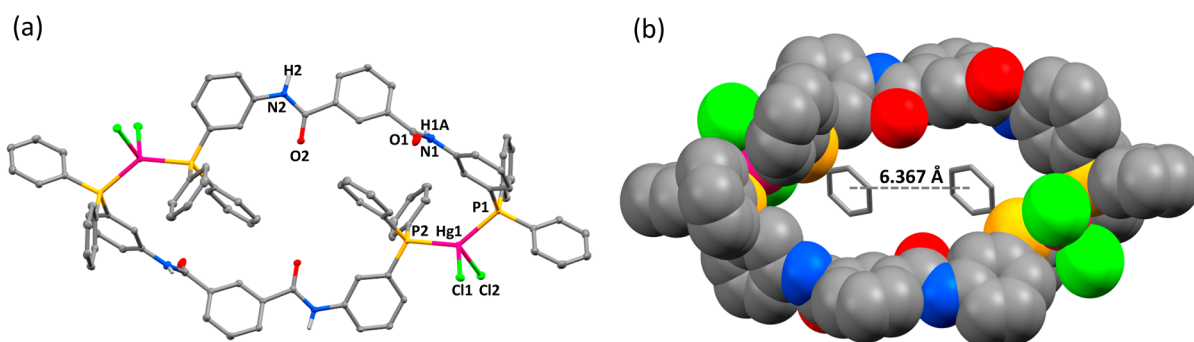


Figure 2. (a) Crystal structure of Hg-macrocyclic **2** where thermal ellipsoids are drawn at the 30% probability level, and hydrogen atoms, except for N–H groups, have been omitted for clarity. Selected bond distances (Å) and bond angles (deg): Hg1–P1, 2.4572 (11); Hg1–P2, 2.4488(11); Hg1–Cl1, 2.5753(11); Hg1–Cl2, 2.5459(11); P2–Hg1–P1, 135.05(4); Cl2–Hg1–Cl1, 105.61(4). (b) Space-fill model of **2** where arene rings bound to the amide groups are shown in a capped stick fashion.

the $P_{\text{phosphine}}$ atoms of two amide-based ligands to constitute a 36-membered cavity. The dimension of this 36-membered cavity was $17.068 \times 6.988 \text{ \AA}^2$ after measuring the distance between pyridine-N \cdots Hg and the two farthest amide-C atoms (Figure S12, Supporting Information). The structure shows that most of the other phenyl groups are not in close contact, therefore leaving the macrocyclic cavity empty. In fact, two amide-bound arene rings are the nearest neighbors with a separation of 5.306 Å, which is certainly outside the range of π – π interactions (Figure 1b).⁷⁰

The crystal structure for Hg-macrocyclic **2**, which is again a 2 + 2 self-assembly, reveals a very different structure wherein both amide functional groups are in anti-conformation (Figure 2). We believe that the absence of a pyridine ring in **2** eliminates the intramolecular H-bonding involving amide N–H groups and that allows free rotation of the amide-based arms and therefore their anti-conformation.⁶⁹ In this case, conformation of two ligands as a result of their coordination to the Hg(II) ions via $P_{\text{phosphine}}$ groups is exocyclic in nature. As a consequence, Hg-bound chloride atoms are faced outside the 32-membered cavity. Further, one phosphine-bound arene ring from each ligand is located inside the macrocyclic cavity. However, both such arene rings do not show any π – π interaction, which is evident from the distance between the two rings, 6.367 Å (Figure 2b).⁷⁰ Interestingly, while two molecules of DMSO were found to crystallize in the lattice, only one of them was involved in H-bonding interactions with the amide group (N1–H1A \cdots O3_{DMSO} = 2.825 Å). Importantly, macrocycle **2** presents a wider cavity than that of **1** which is evident from the dimensions of the cavity: $18.295 \times 10.983 \text{ \AA}^2$ (Figure S13, Supporting Information).

Iodine Inclusion Studies. To understand the probability of guest inclusion within the macrocyclic cavity of **1** and **2**, I₂ inclusion studies were performed. In both cases, an Hg-macrocyclic was evacuated for 1 h at 50 °C in order to remove any adventitious solvent molecule. This was followed by sealing a fixed amount (15.0 mg) of a compound within a glass vial containing solid I₂, and it was allowed to equilibrate with iodine vapors for 2 h. In the case of Hg-macrocyclics **1** and **2**, respectively, a 12.7% (2.2 mg) and 17.1% (3.1 mg) weight change was noted. In both cases, the nearly colorless compound acquired an orange-brown color, suggesting adsorption of molecular iodine within the macrocyclic cavity (Figure S14, Supporting Information). Importantly, the FTIR spectrum of any of the Hg-macrocyclics does not reveal significant changes except for the broadening of the N–H

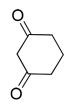
stretches.⁴³ Such a fact points toward the inclusion of I₂ within the cavity of a macrocycle. Notably, the I₂ adsorption process was reversible in nature as the compound regained its original color after a brief evacuation within a minute.

Heterogeneous Catalysis. Both Hg-macrocyclics offered cavities lined with H-bonds which suggest their potential of favorably interacting both with a substrate and a reagent.^{64,65} In addition, both macrocyclics offered cavities of different dimensions and orientations and therefore suggest their propensity to interact with a substrate and/or reagent differently.^{64,65} Furthermore, the presence of Hg(II) ions endows such macrocyclics with Lewis acid character.^{51,53} Considering the aforementioned points, both Hg-macrocyclics provide excellent opportunities to attempt various organic transformations in catalytic fashion. In this context, Knoevenagel condensation reactions (KCRs) were contemplated to be appropriate.^{71,72} This was due to the involvement of O-based substrates that may potentially interact with the N–H groups of the Hg-macrocyclics. In order to evaluate the effect of cavity structure on proposed catalysis and to minimize the influence of solvent molecules, both Hg-macrocyclics were tested as the heterogeneous catalysts.^{71,72}

We initiated KCRs by optimizing the reaction conditions taking Hg-macrocyclic **1** as a representative catalyst and benzaldehyde as a model substrate along with malononitrile as the active methylene reagent while maintaining a reaction time of 4 h (Table 1). The role of Hg-macrocyclic **1** as a catalyst was indispensable as the reaction did not proceed without it (entry 1). Similarly, only ligand and only metal salts (HgCl₂ and Hg(OAc)₂) did not promote the catalytic reaction (entries 2 and 3). The solvent-free reaction was not quite successful due to the lower product yield, despite a reaction time of 12 h, both at milder (30 °C) and higher (60 °C) reaction temperatures (entry 4). We believe that the absence of a solvent led to inadequate mixing of substrate and reagent.

Subsequently, several solvents were scrutinized ranging from nonpolar CH₂Cl₂ to highly polar DMF in addition to MeCN, THF, and MeOH (entry 5). Out of various tested solvents, methanol was found to be the best solvent for promoting KCRs as other solvents resulted in a lower yield of the product. It is suggested that a polar solvent, such as MeOH, is likely to efficiently replace the already existing solvent molecule(s) within the macrocyclic cavity. Such a situation may assist in catalysis by allowing a substrate and/or reagent effectively approaching the Hg-macrocyclic. A very small catalyst loading of 1 mol % was sufficient for promoting the catalytic reactions

Table 1. Optimization Experiments for the Knoevenagel Condensation Reactions^a

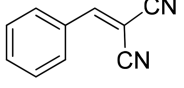
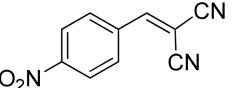
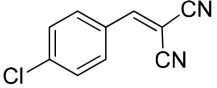
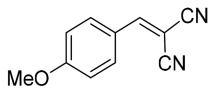
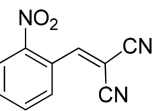
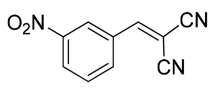
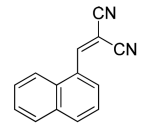
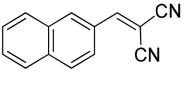
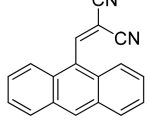
S. No. ^a	Catalyst	R	R'	Solvent	Temp (°C)	Yield (%) ^b
1	--	CN	CN	CH ₃ OH	60	0
2	L1	CN	CN	CH ₃ OH	60	0
3 (a)	HgCl ₂	CN	CN	CH ₃ OH	60	0
(b)	Hg(OAc) ₂	CN	CN	CH ₃ OH	60	0
4	1 ^c	CN	CN	--	30	10
					60	35
5 (a)				CH ₃ OH		>99
(b)				CH ₃ CN		50
(c)	1	CN	CN	CH ₂ Cl ₂	60	10
(d)				THF		75
(e)				DMF		80
6 (a)					0.5	25
(b)	1	CN	CN	0.5	60	45
(c)				1	60	>99
7 (a)	1	CH ₃ CO	CH ₃ CO	CH ₃ OH	60	10
(b)	2	CH ₃ CO	CH ₃ CO	CH ₃ OH	60	10
8 (a)	1					10
(b)	2			CH ₃ OH	60	10
9 (a)				CH ₃ OH		25
(b)				CH ₃ CN		10
(c)	1	CN	COOEt	DCM	60	3
(d)				THF		15
(e)				DMF		25

^aReaction conditions: catalyst: 1-mol %; reaction time: 4 h; temperature: 60 °C. ^bProducts were quantified by using the gas chromatograph. ^cReaction time: 12 h.

quantitatively (entry 6). In addition to malononitrile, other reagents with active methylene groups such as acetylacetone (entry 7), 1,3-cyclohexanedione (entry 8), and ethyl-2-cyanoacetate (entry 9) were also examined. However, none of these reagents were quite effective in promoting KCRs with both the Hg-macrocycles **1** and **2** (vide infra).

These optimized reaction conditions were then utilized to explore catalytic performance with assorted substituted benzaldehydes along with malononitrile (Table 2). Importantly, both the nature of a substituent and its position on benzaldehyde ring had a considerable effect on the product yield.^{42,52} For example, electron-withdrawing groups present at the para position (entries 2 and 3) were much more effective than that at ortho and meta positions (entries 5 and 6) in promoting the catalytic KCRs. In contrast, the electron-donating -OCH₃ group at the para position resulted in a lower product yield (entry 4). To further understand the influence of electronic groups, time-dependent KCRs were carried out for

Table 2. Knoevenagel Condensation Reactions for Assorted Aldehydes along with Malononitrile^a

S. No.	R	Product	Yield (%) ^b	Yield (%) ^b
			1	2
1	C ₆ H ₅		85	99
2	4-NO ₂ C ₆ H ₄ ^c		99	99
3	4-ClC ₆ H ₄		90	99
4	4-MeOC ₆ H ₄		85	90
5	2-NO ₂ C ₆ H ₄		75	99
6	3-NO ₂ C ₆ H ₄		70	80
7	Napthalen-1-yl		80	95
8	Napthalen-2-yl		80	95
9	9-anthracenyl		85	98

^aConditions: catalyst, 1-mol %; solvent, MeOH; reaction time: 4 h; temperature, 60 °C. ^bYield was calculated using the gas chromatograph. ^cReaction was completed within 2 h.

ortho-, meta-, and para-substituted nitro-benzaldehydes with malononitrile (Figure S15, Supporting Information). Importantly, nearly quantitative catalytic reaction was completed within 2 h in the case of *para*-nitro-benzaldehyde, whereas the same reaction took close to 4 h in the case of other two substrates.

More importantly, bulkier substrates were converted to their corresponding products with equally good yields (entries 7–9). In these cases, Hg-macrocycle **2** was found to be a better

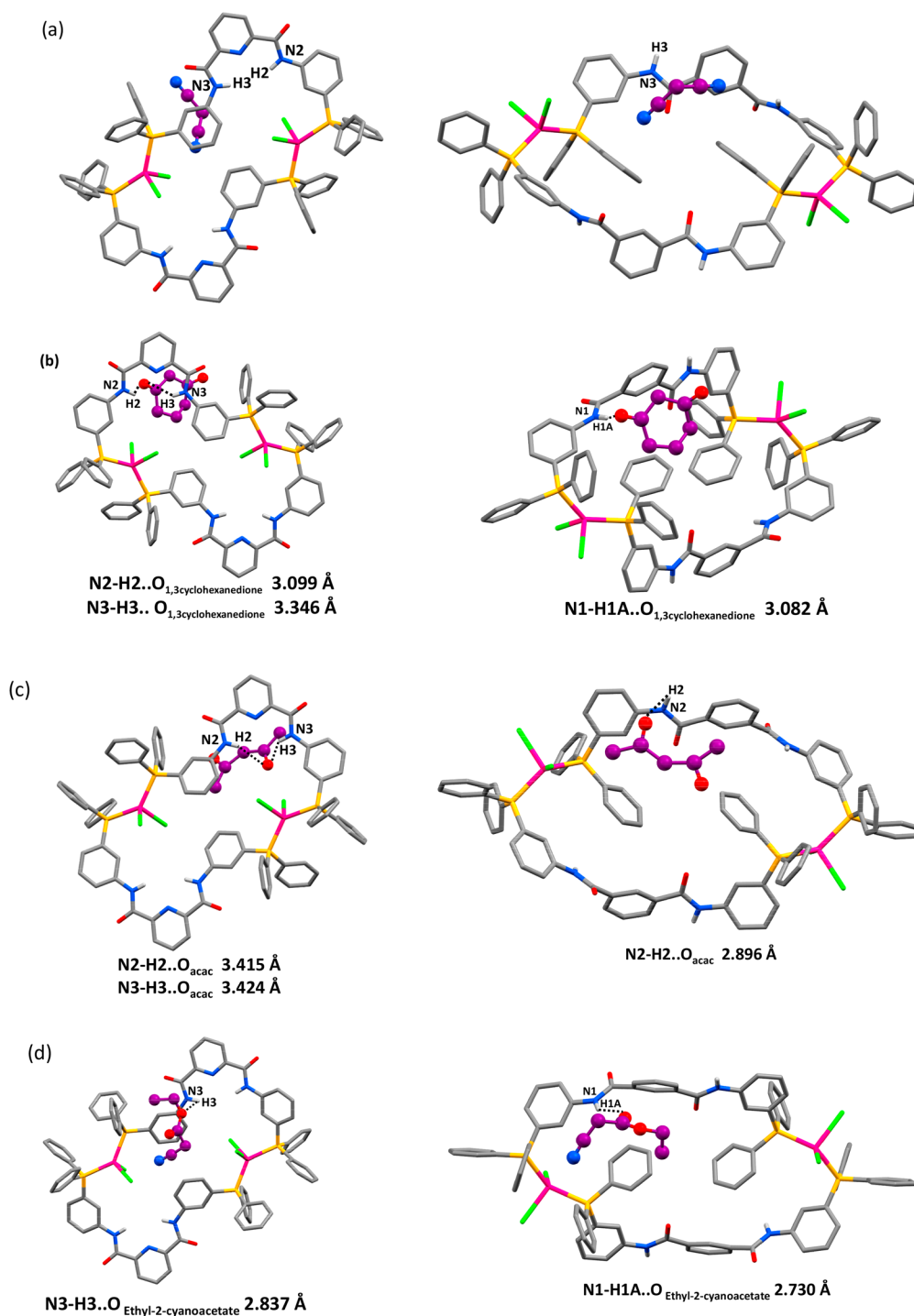


Figure 3. Structures of molecular docking studies for Hg-macrocycles **1** and **2** with the reagents containing active methylene groups: (a) malononitrile; (b) 1,3-cyclohexanedione; (c) acetylacetone; and (d) ethyl-2-cyanoacetate. Hydrogen atoms, except for N–H groups, have been omitted for clarity. Hg-macrocycles **1** and **2** are shown in a capped stick model, whereas reagents are displayed in a ball and stick model where carbon atoms are shown in purple color for the sake of clarity.

catalyst in promoting KCRs when compared to Hg-macrocycle **1**. Such a fact can be nicely correlated to the larger cavity size being offered by Hg-macrocycle **2** when compared to **1**. A comparison between the molecular dimensions of the bulkier substrates (Table S5, Supporting Information)⁷³ 1-naphthaldehyde ($9.69 \times 8.29 \text{ \AA}^2$), 2-naphthaldehyde ($10.67 \times 7.49 \text{ \AA}^2$), and 9-anthraldehyde ($10.88 \times 8.60 \text{ \AA}^2$) to that of the cavity dimensions of Hg-macrocycle **2** ($18.295 \times 10.983 \text{ \AA}^2$) suggests that the cavity is large enough to comfortably accommodate

and therefore activate these substrates. On the other hand, Hg-macrocycle **1** presents a slightly smaller macrocyclic cavity ($17.068 \times 6.988 \text{ \AA}^2$), and therefore bulkier substrates may have difficulty in being comfortably accommodated within the cavity.

Docking Studies. As discussed (cf. Table 1), KCRs were performed with four different reagents containing active methylene groups malononitrile, 1,3-cyclohexanedione, acetylacetone, and ethyl-2-cyanoacetate. Out of four reagents, only

malononitrile provided a high yield of the products with a variety of substituted benzaldehydes, while the remaining three reagents were largely ineffective. To gain insight about the difference in their reactivity, molecular docking studies were performed.^{66,74} These studies may help us in understanding the role of H-bonding in accommodating and plausibly retaining such substrates within the macrocyclic cavities. Importantly, malononitrile was not found to form any H-bonds within the macrocyclic cavity (Figure 3a) and therefore was freely available to react with the benzaldehyde. As a result, malononitrile provided a very high yield of the KCR product. On the other hand, remaining three substrates 1,3-cyclohexanedione, acetylacetone, as well as ethyl-2-cyanoacetate were involved in many H-bonding interactions within the macrocyclic cavities. For example, the O atom of 1,3-cyclohexanedione was noted to form H-bond(s) with the N–H group(s) of the Hg-macrocycles (Figures 3b and S16, Supporting Information). Similarly, acetylacetone also interacted with the cavity via N–H...O synthons (Figures 3c, S17 and S18, Supporting Information). Finally, ethyl-2-cyanoacetate was also seen interacting with the N–H groups of the cavities. In this case, two types of H-bonding synthons were observed: N–H...O and N–H...NC interactions (Figures 3d, S19, S20, and S21, Supporting Information).

Such studies suggest that 1,3-cyclohexanedione, acetylacetone, and ethyl-2-cyanoacetate were involved in many H-bonding interactions within the cavity of a Hg-macrocyclic. We propose that such a fact retains or locks a reagent within an Hg-macrocyclic and substantially reduces its reactivity with a substrate, such as benzaldehyde. To prove the above hypothesis, FTIR spectra of Hg-macrocyclics impregnated with these reagents were measured. Notably, in all three cases (1,3-cyclohexanedione, acetylacetone, and ethyl-2-cyanoacetate), N–H stretches of the Hg-macrocyclics were significantly red-shifted when compared to the pristine samples of Hg-macrocyclics. A representative FTIR spectrum of Hg-macrocyclic 2 impregnated with acetylacetone illustrates that N–H stretches of 2 were shifted from 3271 to 3254 cm^{-1} . Such a fact asserts the interaction and potential locking of acetylacetone within the macrocyclic cavity (Figure S22, Supporting Information).⁴¹

We also evaluated the potential activation of a substrate (benzaldehyde) within the cavity of the present Hg-macrocyclics by taking 2 as a representative case. For such an experiment, a vacuum-dried (at 50 °C) sample of 2 was dipped in a CH_2Cl_2 solution of benzaldehyde for 2 h and the said impregnated sample was filtered, washed thoroughly with CH_2Cl_2 , and vacuum-dried. This impregnated sample showed red-shifted stretches for the C=O group of benzaldehyde, from 1705 to 1676 cm^{-1} , in the FTIR spectrum (Figure S23, Supporting Information).^{42,50} In addition, N–H stretches of the Hg-macrocyclics were also perturbed after the inclusion of benzaldehyde. This experiment therefore asserts that benzaldehyde has been indeed accommodated within the macrocyclic cavity and thus has been activated. We propose that both Lewis acid activation and H-bonding interaction contribute here.

Recyclability Experiments. The importance of a heterogeneous catalyst lies in its ability to be recycled and reused.⁷⁵ Therefore, in order to justify the heterogeneous nature of the present catalysts, Hg-macrocyclic 2 was selected as a model catalyst for the hot filtration experiment during the course of a reaction between benzaldehyde and malononitrile (Figure

4a).^{40,43} If a KCR is allowed uninterrupted, then nearly quantitative product formation is noted at the end (blue

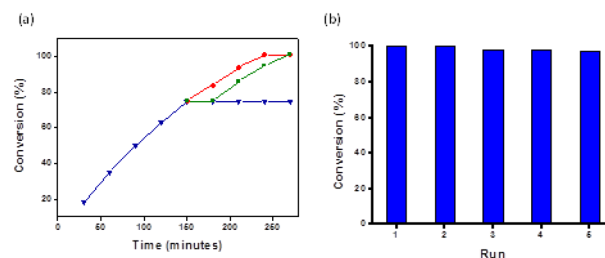


Figure 4. (a) Hot-filtration test for the Knoevenagel condensation reaction between benzaldehyde and malononitrile in the presence of Hg-macrocyclic 2. Catalyst 2 was filtered off at 150 min (blue triangles) and readded at 175 min (green squares). (b) Bar graph displaying recyclability of Hg-macrocyclic 2 for five consecutive cycles.

triangle and red dots). Notably, the catalytic reaction comes to an end as soon as the catalyst is filtered off from the reaction mixture at 150 min. As expected, there is no further reaction without the catalyst (blue triangles). Readdition of the catalyst at 175 min restarts the catalysis, and the reaction leads to completion (green squares). Thus, this simple filtration test confirms the true heterogeneous nature of the catalysis.

Additional evidence was obtained by analyzing the filtrates of the KCR after removing Hg-macrocyclic 1 by using the atomic absorption spectroscopy-visual gas analyzer (AAS-VGA). The amount of mercury leached from Hg-macrocyclic 1 into the filtrate was only 0.0036% and 0.0479% after 4 and 24 h, respectively. This experiment thus eliminates the appreciable leaching of mercury from Hg-macrocyclics and supports their stable nature as the heterogeneous catalysts.

Importantly, recovered Hg-macrocyclics would certainly allow exploring their recyclability.^{42–47} For such studies, Hg-macrocyclic 2 was selected as a representative catalyst in a reaction of benzaldehyde with malononitrile. Importantly, Hg-macrocyclic 2 was recovered by simple filtration and was successfully used for five consecutive cycles without any further purification and/or activation.^{42–47} In all such cycles, no noticeable change in the catalytic performance was observed (Figure 4b).

More importantly, both Hg-macrocyclics were isolated after their fifth catalytic cycle and characterized by the FTIR spectra. FTIR spectra exhibited superimposable traces of the recovered Hg-macrocyclics to that of pristine samples (Figures S24 and S25, Supporting Information). Similarly, powder XRD patterns of the recovered Hg-macrocyclics matched nicely to that of as-synthesized samples (Figures S26 and S27, Supporting Information). Such a fact asserts that both Hg-macrocyclics maintained their crystallinity as well as structural integrity during the catalysis. Collectively, these studies sufficiently support the robust nature of both Hg-macrocyclics as the heterogeneous catalysts.

Conclusion. This work described the synthesis and characterization of two Hg-macrocyclics 1 and 2 offering H-bonding based cavities of varying dimensions. Crystal structures illustrated remarkable influence of the presence (in 1) or absence (in 2) of pyridine-2,6-dicarboxamide based fragment in controlling the macrocyclic cavity structure. Such a structural feature resulted in a noteworthy difference in the heterogeneous catalytic performance of two Hg-macrocyclics in Knoevenagel condensation reactions (KCRs). The catalytic

results illustrated two notable trends: (i) Hg-macrocyclic **2** having phenylene ring functioned as a much effective catalyst when compared to Hg-macrocyclic **1** with the pyridyl ring; and (ii) except malononitrile, remaining three reagents were largely ineffective in promoting KCRs. The first trend was related to the cavity dimensions being offered by the two Hg-macrocyclic where it was concluded that **2**, offering larger cavity, was able to activate both a substrate (benzaldehyde) and a reagent (malononitrile) better than that of **1**. The difference between various reagents (malononitrile, 1,3-cyclohexanedione, acetylacetone, and ethyl-2-cyanoacetate) was related to the locking of a reagent within the macrocyclic cavity due to the involvement of H-bonding interactions. These results were well-supported by the molecular docking studies and FTIR spectral studies. Future work is directed to modify the macrocyclic cavity structure to relate to the catalysis of challenging organic transformations.

■ ASSOCIATED CONTENT

Supporting Information

The Supporting Information is available free of charge on the ACS Publications website at DOI: [10.1021/acs.cgd.9b00999](https://doi.org/10.1021/acs.cgd.9b00999).

Experimental section and figures for the FTIR and NMR spectra, TGA, powder XRD patterns, molecular docking studies, I₂ adsorption studies, time-profile for a KCR, and tables for the molecular dimensions of various substrates, crystallographic data collection, and bonding parameters (PDF)

Accession Codes

CCDC [1943636](https://doi.org/10.1021/1943636)–[1943637](https://doi.org/10.1021/1943637) contain the supplementary crystallographic data for this paper. These data can be obtained free of charge via www.ccdc.cam.ac.uk/data_request/cif, or by emailing data_request@ccdc.cam.ac.uk, or by contacting The Cambridge Crystallographic Data Centre, 12 Union Road, Cambridge CB2 1EZ, UK; fax: +44 1223 336033.

■ AUTHOR INFORMATION

Corresponding Author

*E-mail: rgupta@chemistry.du.ac.in. Website: <http://people.du.ac.in/~rgupta/>.

ORCID

Rajeev Gupta: [0000-0003-2454-6705](https://orcid.org/0000-0003-2454-6705)

Notes

The authors declare no competing financial interest.

■ ACKNOWLEDGMENTS

R.G. acknowledges financial support from the Science and Engineering Research Board, New Delhi (EMR/2016/000888). S.P. thanks UGC, New Delhi, for her fellowship. The authors thank the University of Delhi for the instrumental facilities including X-ray data collection.

■ REFERENCES

- (1) Lescop, C. Coordination-Driven Syntheses of Compact Supramolecular Metallacycles toward Extended Metallo-organic Stacked Supramolecular Assemblies. *Acc. Chem. Res.* **2017**, *50*, 885–894.
- (2) Northrop, B. H. Coordination-driven self-assembly of functionalized supramolecular metallacycles. *Chem. Commun.* **2008**, 5896–5908.

- (3) Cook, T. R.; Stang, P. J. Recent Developments in the Preparation and Chemistry of Metallacycles and Metallacages via Coordination. *Chem. Rev.* **2015**, *115*, 7001–7045.

- (4) Chen, L.; Chen, Q.; Wu, M.; Jiang, F.; Hong, M. Controllable Coordination-Driven Self-Assembly: From Discrete Metallacages to Infinite Cage-Based Frameworks. *Acc. Chem. Res.* **2015**, *48*, 201–210.

- (5) Kumar, G.; Gupta, R. Molecularly designed architectures – the metalloligand way. *Chem. Soc. Rev.* **2013**, *42*, 9403–9453.

- (6) Lindoy, L. F.; Park, K. M.; Lee, S. S. Metals, Macrocycles and Molecular Assemblies - Macrocyclic Complexes in Metallo-Supramolecular Chemistry. *Chem. Soc. Rev.* **2013**, *42*, 1713–1727.

- (7) Seidel, S. R.; Stang, P. J. High-Symmetry Coordination Cages via Self-Assembly. *Acc. Chem. Res.* **2002**, *35*, 972–983.

- (8) Li, B.; He, T.; Fan, Y.; Yuan, X.; Qiu, H.; Yin, S. Recent developments in the construction of metallacycle/metallacage-cored supramolecular polymers via hierarchical self-assembly. *Chem. Commun.* **2019**, 55, 8036–8059.

- (9) Wang, W.; Wang, Y. S.; Yang, H. B. Supramolecular transformations within discrete coordination-driven supramolecular architectures. *Chem. Soc. Rev.* **2016**, *45*, 2656–2693.

- (10) Singh, A. P.; Ali, A.; Gupta, R. Cobalt complexes as the building blocks: {Co³⁺-Zn²⁺} heterobimetallic networks and their properties. *Dalton Trans* **2010**, 39, 8135–8138.

- (11) Mishra, A.; Gupta, R. Supramolecular architecture with pyridine-amide based ligands: discrete molecular assemblies and their applications. *Dalton Trans* **2014**, 43, 7668–7682.

- (12) Wei, P.; Yan, X.; Huang, F. Supramolecular polymers constructed by orthogonal self-assembly based on host–guest and metal–ligand interactions. *Chem. Soc. Rev.* **2015**, *44*, 815–832.

- (13) Brown, C. J.; Toste, F. D.; Bergman, R. G.; Raymond, K. N. Supramolecular Catalysis in Metal–Ligand Cluster Hosts. *Chem. Rev.* **2015**, *115*, 3012–3035.

- (14) Cram, D. J. Molecular container compounds. *Nature* **1992**, *356*, 29–36.

- (15) Zhou, J.; Yu, G.; Huang, F. Supramolecular chemotherapy based on host–guest molecular recognition: a novel strategy in the battle against cancer with a bright future. *Chem. Soc. Rev.* **2017**, *46*, 7021–7053.

- (16) Yu, G.; Han, C.; Zhang, Z.; Chen, J.; Yan, X.; Zheng, B.; Liu, S.; Huang, F. Pillar[6]arene-Based Photoresponsive Host–Guest Complexation. *J. Am. Chem. Soc.* **2012**, *134*, 8711–8717.

- (17) Tanner, M. E.; Knobler, C. B.; Cram, D. J. Rigidly Hollow Hosts That Encapsulate Small Molecules. *J. Org. Chem.* **1992**, *57*, 40–46.

- (18) Dong, V. M.; Fiedler, D.; Carl, B.; Bergman, R. G.; Raymond, K. N. Molecular Recognition of Iminium Ions in Water. *J. Am. Chem. Soc.* **2006**, *128*, 14464–14465.

- (19) Lésniewska, B.; Coleman, A. W.; Perret, F.; Suwinska, K. Tuning Solid-State Calix[n]arene Supramolecular Assemblies Using Phenanthroline as the Guest Molecule. *Cryst. Growth Des.* **2019**, *19*, 1695–1708.

- (20) Purba, P. C.; Bhattacharyya, S.; Maity, M.; Mukhopadhyay, S.; Howlader, P.; Mukherjee, P. S. Linkage induced enhancement of fluorescence in metal–carbene bond directed metallacycles and metallacages. *Chem. Commun.* **2019**, 55, 8309–8312.

- (21) Wang, P.; Yao, Y.; Xue, M. A novel fluorescent probe for detecting paraquat and cyanide in water based on pillar[5]arene/10-methylacridinium iodide molecular recognition. *Chem. Commun.* **2014**, *50*, 5064–5067.

- (22) Qi, Z.; Heinrich, T.; Moorthy, S.; Schalley, C. S. Gas-phase chemistry of molecular containers. *Chem. Soc. Rev.* **2015**, *44*, 515–531.

- (23) Yao, L. Y.; Qin, L.; Xie, T. Z.; Li, Y. Z.; Yu, S. Y. Synthesis and Anion Sensing of Water-Soluble Metallomacrocycles. *Inorg. Chem.* **2011**, *50*, 6055–6062.

- (24) Das, P.; Kumar, A.; Chowdhury, A.; Mukherjee, P. S. Aggregation-Induced Emission and White Luminescence from a Combination of π -Conjugated Donor-Acceptor Organic Luminogens. *ACS Omega* **2018**, *3*, 13757–13771.

- (25) Xu, L.; Wang, Y. X.; Yang, H. B. Recent Advances in the construction of fluorescent metallacycles and metallocages via coordination-driven assembly. *Dalton Trans* **2015**, *44*, 867–890.
- (26) Guzman-Percestequi, E.; Vonlanthen, M.; Quiroz-Garcia, B.; Flores-Alamo, M.; Rivera, E.; Castillo, I. Supramolecular Fluorescence Enhancement via Coordination Driven Self-Assembly in Rigid bis-Picolylcalixarene-derived Blue Emitting $M_2L_2X_n$ Macrocycles. *Dalton Trans* **2015**, *44*, 15966–15975.
- (27) Webber, M. J.; Langer, R. Drug delivery by supramolecular design. *Chem. Soc. Rev.* **2017**, *46*, 6600–6620.
- (28) Ma, D.; Hettiarachchi, G.; Nguyen, D.; Zhang, B.; Wittenberg, J. B.; Zavalij, P. Y.; Briken, V.; Isaacs, L. Acyclic cucurbit[n]uril molecular containers enhance the solubility and bioactivity of poorly soluble pharmaceuticals. *Nat. Chem.* **2012**, *4*, 503–510.
- (29) Plumb, J. A.; Venugopal, B.; Oun, R.; Gomez-Roman, N.; Kawazoe, Y.; Venkataraman, N. S.; Wheate, N. J. Cucurbit[7]uril encapsulated cisplatin overcomes cisplatin resistance via a pharmacokinetic effect. *Metallomics* **2012**, *4*, 561–567.
- (30) Mejia-Ariza, R.; Grana-Suárez, L.; Verboom, W.; Huskens, J. Cyclodextrin-based supramolecular nanoparticles for biomedical applications. *J. Mater. Chem. B* **2017**, *5*, 36–52.
- (31) Duan, Q.; Cao, Y.; Li, Y.; Hu, X.; Xiao, T.; Lin, C.; Pan, Y.; Wang, L. pH-Responsive Supramolecular Vesicles Based on Water-Soluble Pillar[6]arene and Ferrocene Derivative for Drug Delivery. *J. Am. Chem. Soc.* **2013**, *135*, 10542–10549.
- (32) Loh, X. J. Supramolecular host–guest polymeric materials for biomedical applications. *Mater. Horiz.* **2014**, *1*, 185–195.
- (33) Giuliani, M.; Morbioli, I.; Sansone, F.; Casnati, A. Moulding calixarenes for biomacromolecule targeting. *Chem. Commun.* **2015**, *51*, 14140–14159.
- (34) Rajora, M. A.; Lou, J. W. H.; Zheng, G. Advancing porphyrin's biomedical utility via supramolecular chemistry. *Chem. Soc. Rev.* **2017**, *46*, 6433–6469.
- (35) Gandara-Loe, J.; Ortuño-Lizarán, I.; Fernández-Sánchez, L.; Alió, J. L.; Cuenca, N.; Vega-Estrada, A.; Silvestre-Albero, J. Metal–Organic Frameworks as Drug Delivery Platforms for Ocular Therapeutics. *ACS Appl. Mater. Interfaces* **2019**, *11*, 1924–1931.
- (36) Marsault, E.; Peterson, M. L. Macrocycles Are Great Cycles: Applications, Opportunities, and Challenges of Synthetic Macrocycles in Drug Discovery. *J. Med. Chem.* **2011**, *54*, 1961–2004.
- (37) Galan, A.; Ballester, P. Stabilization of reactive species by supramolecular encapsulation. *Chem. Soc. Rev.* **2016**, *45*, 1720–1737.
- (38) Fiedler, D.; Bergman, R. G.; Raymond, K. N. Stabilization of Reactive Organometallic Intermediates inside a Self Assembled Nanoscale Host. *Angew. Chem., Int. Ed.* **2006**, *45*, 745–748.
- (39) Eelkema, R.; Maeda, K.; Odell, B.; Anderson, H. L. Radical Cation Stabilization in a Cucurbituril Oligoaniline Rotaxane. *J. Am. Chem. Soc.* **2007**, *129*, 12384–12385.
- (40) Pandey, S.; Bansal, D.; Gupta, R. A Metalloligand Appended with Benzimidazole Rings: Tetranuclear $[CoZn_3]$ and $[CoCd_3]$ Complexes and Their Catalytic Applications. *New J. Chem.* **2018**, *42*, 9847–9856.
- (41) Liu, Y.; Zhang, R.; He, C.; Dang, D.; Duan, C. A palladium(II) triangle as building blocks of microporous molecular materials: structures and catalytic performance. *Chem. Commun.* **2010**, *46*, 746–748.
- (42) Srivastava, S.; Kumar, V.; Gupta, R. A Carboxylate-Rich Metalloligand and Its Heterometallic Coordination Polymers: Synthesis, Structures, Topologies and Heterogeneous Catalysis. *Cryst. Growth Des.* **2016**, *16*, 2874–2886.
- (43) Kumar, G.; Hussain, F.; Gupta, R. Carbon-sulphur cross coupling reactions catalyzed by nickel-based coordination polymers based on metalloligands. *Dalton Trans* **2017**, *46*, 15023–15031.
- (44) Kumar, G.; Kumar, G.; Gupta, R. Manganese and Cobalt-Based Coordination Networks as Promising Heterogeneous Catalysts for Olefin Epoxidation Reactions. *Inorg. Chem.* **2015**, *54*, 2603–2615.
- (45) Kumar, G.; Gupta, R. Three-Dimensional $\{Co^{3+}-Zn^{2+}\}$ and $\{Co^{3+}-Cd^{2+}\}$ Networks Originated from Carboxylate-rich Building Blocks: Syntheses, Structures, and Heterogeneous Catalysis. *Inorg. Chem.* **2013**, *52*, 10773–10787.
- (46) Kumar, G.; Kumar, G.; Gupta, R. Lanthanide-based coordination polymers as promising heterogeneous catalysts for ring-opening reactions. *RSC Adv.* **2016**, *6*, 21352–21361.
- (47) Kumar, G.; Gupta, R. Cobalt Complexes Appended with p- and m-Carboxylates: Two Unique $\{Co^{3+}-Cd^{2+}\}$ Networks and Their Regioselective and Size-Selective Heterogeneous Catalysis. *Inorg. Chem.* **2012**, *51*, 5497–5499.
- (48) Samanta, D.; Mukherjee, S.; Patil, Y. P.; Mukherjee, P. S. Self-Assembled Pd₆ Open Cage with Triimidazole Walls and the Use of Its Confined Nanospace for Catalytic Knoevenagel- and Diels–Alder Reactions in Aqueous Medium. *Chem.–Eur. J.* **2012**, *18*, 12322–12329.
- (49) Srivastava, S.; Dagur, M. S.; Ali, A.; Gupta, R. Trinuclear $\{Co^{2+}-M^{3+}-Co^{2+}\}$ complexes catalyze reduction of nitro compounds. *Dalton Trans* **2015**, *44*, 17453–17461.
- (50) Pandey, S.; Kumar, G.; Gupta, R. Postfunctionalized Metalloligand-Based Catenated Coordination Polymers: Syntheses, Structures, and Effect of Labile Sites on Catalysis. *Cryst. Growth Des.* **2019**, *19*, 2723–2735.
- (51) Mishra, A.; Ali, A.; Upreti, S.; Gupta, R. Cobalt Coordination Induced Functionalized Molecular Clefs: Isolation of $\{Co^{III}-Zn^{II}\}$ Heterometallic Complexes and Their Applications in Beckmann Rearrangement Reactions. *Inorg. Chem.* **2008**, *47*, 154–161.
- (52) Bansal, D.; Pandey, S.; Hundal, G.; Gupta, R. Heterometallic coordination polymers: syntheses, structures and heterogeneous catalytic applications. *New J. Chem.* **2015**, *39*, 9772–9781.
- (53) Mishra, A.; Ali, A.; Upreti, S.; Whittingham, M. S.; Gupta, R. Cobalt complex as building blocks: synthesis, characterization, and catalytic applications of $\{Cd^{2+}-Co^{3+}-Cd^{2+}\}$ and $\{Hg^{2+}-Co^{3+}-Hg^{2+}\}$ heterobimetallic complexes. *Inorg. Chem.* **2009**, *48*, 5234–5243.
- (54) Stang, P. J.; Olenyuk, B. Self-Assembly, Symmetry, and Molecular Architecture: Coordination as the Motif in the Rational Design of Supramolecular Metallacyclic Polygons and Polyhedra. *Acc. Chem. Res.* **1997**, *30*, 502–518.
- (55) Yoshizawa, M.; Klosterman, J. K.; Fujita, M. Functional Molecular Flasks: New Properties and Reactions within Discrete, Self-Assembled. *Angew. Chem., Int. Ed.* **2009**, *48*, 3418–3438.
- (56) Fujita, M.; Tominaga, M.; Hori, A.; Therrien, B. Coordination Assemblies from a Pd(II)-Cornered Square Complex. *Acc. Chem. Res.* **2005**, *38*, 369–378.
- (57) Olenyuk, B.; Fechtenkötter, A.; Stang, P. J. Molecular architecture of cyclic nanostructures: use of co-ordination chemistry in the building of supermolecules with predefined geometric shapes. *J. Chem. Soc., Dalton Trans.* **1998**, 1707–1728.
- (58) Chakrabarty, R.; Mukherjee, P. S.; Stang, P. J. Supramolecular Coordination: Self-Assembly of Finite Two- and Three-Dimensional Ensembles. *Chem. Rev.* **2011**, *111*, 6810–6918.
- (59) Tong, J.; Jia, L. M.; Shang, P.; Yu, S. Y. Controlled Synthesis of Supramolecular Architectures of Homo- and Heterometallic Complexes by Programmable Self-Assembly. *Cryst. Growth Des.* **2019**, *19*, 30–39.
- (60) Caulder, D. L.; Raymond, K. N. Supermolecules by Design. *Acc. Chem. Res.* **1999**, *32*, 975–982.
- (61) Burchell, T. J.; Eisler, D. J.; Puddephatt, R. J. Self-Assembly Using Dynamic Coordination Chemistry and Hydrogen Bonding: Mercury(II) Macrocycles, Polymers and Sheets. *Inorg. Chem.* **2004**, *43*, 5550–5557.
- (62) Nasser, N.; Borecki, A.; Boyle, P. D.; Puddephatt, R. J. A Versatile Diphosphine Ligand: cis and trans Chelation or Bridging, with Self Association through Hydrogen Bonding. *Inorg. Chem.* **2013**, *52*, 7051–7060.
- (63) Marshall, L. J.; de Mendoza, J. Self-Assembled Squares and Triangles by Simultaneous Hydrogen Bonding and Metal Coordination. *Org. Lett.* **2013**, *15*, 1548–1551.
- (64) Casnati, A.; Sansone, F.; Ungaro, R. Peptido- and Glycolcalixarenes: Playing with Hydrogen Bonds around Hydrophobic Cavities. *Acc. Chem. Res.* **2003**, *36*, 246–254.

(65) Adriaenssens, L.; Ballester, P. Hydrogen bonded supra-molecular capsules with functionalized interiors: the controlled orientation of included guests. *Chem. Soc. Rev.* **2013**, *42*, 3261–3277.

(66) Kumar, S.; Kishan, R.; Kumar, P.; Pachisia, S.; Gupta, R. Size-Selective Detection of Picric Acid by Fluorescent Palladium Macrocycles. *Inorg. Chem.* **2018**, *57*, 1693–1697.

(67) (a) Nakamoto, K. *Infrared and Raman Spectra of Inorganic and Coordination Compounds: Part A: Theory and Applications in Inorganic Chemistry*, John Wiley & Sons, Inc., 6th ed., 2008. (b) Nakamoto, K. *Infrared and Raman Spectra of Inorganic and Coordination compounds: Part B: Theory and Applications in Inorganic Chemistry*, John Wiley & Sons, Inc., 6th ed., 2008.

(68) Yang, L.; Powell, D. R.; Houser, R. P. Structural variation in copper(I) complexes with pyridylmethylamide ligands: structural analysis with a new four-coordinate geometry index, τ_4 . *Dalton Trans.* **2007**, 955–964.

(69) Kumar, P.; Gupta, R. The wonderful world of pyridine-2,6-dicarboxamide based scaffolds. *Dalton Trans* **2016**, *45*, 18769–18783.

(70) Martinez, C. R.; Iverson, B. L. Rethinking the term “pi-stacking”. *Chem. Sci.* **2012**, *3*, 2191–2201.

(71) Freeman, F. Properties and Reactions of Ylidenemalononitriles. *Chem. Rev.* **1980**, *80*, 329–350.

(72) Srivastava, S.; Ali, A.; Tyagi, A.; Gupta, R. $\{Cu^{2+}-Co^{3+}-Cu^{2+}\}$ and $\{Cu^{2+}-Fe^{3+}-Cu^{2+}\}$ Heterobimetallic Complexes and Their Catalytic Properties. *Eur. J. Inorg. Chem.* **2014**, *2014*, 2113–2123.

(73) Hasegawa, S.; Horike, S.; Matsuda, R.; Furukawa, S.; Mochizuki, K.; Kinoshita, Y.; Kitagawa, S. Three-Dimensional Porous Coordination Polymer Functionalized with Amide Groups Based on Tridentate Ligand: Selective Sorption and Catalysis. *J. Am. Chem. Soc.* **2007**, *129*, 2607–2614.

(74) A few relevant conformations, with the lowest energies, were selected for evaluating the interaction(s) of a substrate within the cavity of a Hg-macrocycle.

(75) Cai, Q.; Liang, G.; Xu, Y.; Qian, X.; Zhu, W. A Reusable Heterogeneous Catalyst without Leaking Palladium for Highly-Efficient Suzuki-Miyaura Reaction in Pure Water under Air. *RSC Adv.* **2016**, *6*, 60996–61000.